

Stereographic Projection Diffusion Monte Carlo (SPDMC) Algorithms for Molecular Condensed Matter

Michael W. Avilés and E. Curotto*

Department of Chemistry and Physics, Arcadia University, Glenside, Pennsylvania 19038-3295

Received: October 17, 2006; In Final Form: January 18, 2007

We develop and test three algorithms for diffusion Monte Carlo simulations in non-Euclidean manifolds. The methods are based on the construction of the “velocity” distribution by rejection techniques and are capable of functioning in a broad class of non-Euclidean spaces generated by holonomic constraints. The formulation of the propagator for non-Euclidean manifolds avoids the use of Lagrange multipliers; it is derived instead from the Feynman quantization in manifolds proposed by DeWitt. The manifolds are mapped onto \mathbb{R}^d by using stereographic projection coordinates. Numerical tests are conducted for the particle in a ring of unit radius subjected to a sinusoidal potential, for the electron in the field of an infinitely massive proton, and for a water molecule modeled as an asymmetric top subjected to an external field.

1. Introduction

Diffusion Monte Carlo (DMC) is a stochastic algorithm¹ used to determine, in general, the ground state wavefunction and energy of quantum systems. DMC exploits the isomorphism between the (imaginary) time dependent Schrödinger equation and the diffusion equation in the Euclidean space of equal dimension. The potential energy surface plays the role of a sink or source for the diffusion process. The original formulation by Anderson¹ is an algorithm that simulates the diffusion of a number N of replicas of a physical particle (called psips) using a two part strategy. The popularity of the DMC approach² is likely the result of its simple implementation, and its linear scalability with dimension. DMC finds two main applications in theoretical chemistry. It is frequently used to calculate the ground electronic state of atoms and molecules.^{3–5} The particle statistics, which give rise to the Pauli exclusion principle, are often accounted for with approximations. Usually, the location of the nodal surface is found by other first-principle approximations; the DMC solution is exact for bosonic systems. The second popular application is found in condensed matter physics, where nuclear motion is quantized^{6–8} and the ground state^{9–11} for a number of atoms (and/or weakly bound molecules) is required. For both of these applications, the literature is voluminous, and the cited references are only a representative sample. It is more difficult to obtain information about the excited states of a quantum system with DMC; however, progress^{12,13} along these lines has been reported.

Cartesian coordinates yield the simplest quantum Monte Carlo algorithms; however, Cartesian coordinates are too limiting for applications in important problems in molecular physics. Of particular interest to us is the simulation of condensed matter with theories that demand the use of non-Euclidean spaces. Chief among these theories are those that make use of holonomic constraints to handle disparate time scales. There are several kinds of constraints that are often important in molecular physics. Examples difficult to handle with Cartesian coordinates alone are simulations of aggregates of covalent non-linear molecules. The covalent stretches have a characteristic frequency

typically larger by 1 or 2 orders of magnitude compared to the intermolecular degrees of freedom. A number of empirical potential energy surface models capable of achieving spectroscopic precision treat high-frequency degrees of freedom quantum mechanically.⁹

In a number of works we have learned that the disparate time scales have a profound impact on the convergence of quantum Monte Carlo methods like DMC.^{14–18} Using both simple models and molecular clusters, we have shown that using holonomic constraints can increase the efficiency of path integral simulations by orders of magnitude at temperatures below which high degrees of freedom are predominantly in the ground state. The improvement in efficiency that can be gained by using holonomic constraints has been recognized by the community. We are aware of two methods that have been developed to treat diffusion Monte Carlo simulations in non-Euclidean spaces. The first one is by Sarsa et al.,⁷ in their work, the forces of constraint are obtained classically using a set of Lagrange multipliers. The multipliers are calculated at every time step. The resulting forces of constraint are added to the classical Langevin equation in Cartesian coordinates. The integration of the latter over the time step produces an additional drift term for the diffusion process. The clear importance of the advance made by Sarsa et al.⁷ is reflected by the number of growing applications of their method.^{19–22} The second class of methods is by Buch,⁶ where rotations are treated by vector spaces. The theory used by Buch⁶ is more general, as it is applicable to cosets that arise from holonomic constraints. The method developed by Buch⁶, however, requires vector spaces. Recently, other groups have made use of generalizations of the DMC algorithm to differentiable manifolds. In particular, work on the fixed-phase simulation of the fractional quantum Hall effect on the Haldane sphere²³ using stereographic projection coordinates^{24,25} has led to advances related to the one we propose here for molecular dynamics.

Therefore, we are driven to seek general, more efficient methods for DMC simulations of molecular systems in non-Euclidean spaces. The methods we propose in this Article circumvent the calculation of Lagrange multipliers and avoid the use of vector spaces. To see how DMC methods in

* Corresponding author.

alternative coordinates can be superior to the methods available presently, one needs to consider the problem of finding the ground state of the water octamer. One would need to compute 24 Lagrange multipliers at every propagation step for every replica and run a simulation in 72 dimensions. For the water octamer, the methods reported here cost as much as a 48 dimensional simulation without the need to optimize multipliers at every step.

The present Article is a summary of our efforts to extend DMC to manifolds relevant to molecular dynamics mapped with stereographic projection coordinates.^{24,25} In section 2 we present the general theory. For brevity, we omit the derivations of Φ , and the metric tensor $g_{\mu\nu}$ on all these spaces except for \mathbb{R}^d . Derivations of these quantities for various molecular simulations can be found in a number of recent articles.^{14–17} Section 3 contains our results. Numerous simulations for the particle in a ring of unit radius subjected to a sinusoidal potential, and for the electron in the field of an infinitely massive proton are used to confirm that the approaches we develop in section 2 converge. To illustrate the power of the algorithms, we simulate a molecule in an external field using a rigid asymmetric ellipsoid of inertia space. This last example is non-trivial to solve with conventional methods. Finally, section 4 contains discussions and conclusions.

2. Method

In DMC simulations, the time-dependent Schrödinger equation in \mathbb{R}^d

$$-i\hbar \frac{\partial \psi}{\partial t} = \frac{\hbar^2}{2m} \nabla^2 \psi - V\psi \quad (1)$$

is solved for the ground state energy and wavefunction by propagating in imaginary time $\tau = it$. In imaginary time, the time-dependent Schrödinger equation in \mathbb{R}^d is isomorphic to a diffusion equation with the potential energy surface acting as a source-sink of “particles”. In the original DMC approach by Anderson,¹ the particles (called psips) are replicas of the physical particle(s). These replicas are made to move in configuration space by an amount Δx chosen from a Gaussian distribution

$$W(\Delta x) = \sqrt{\frac{m}{2\pi\hbar\Delta\tau}} \exp\left\{-\frac{m(\Delta x)^2}{2\hbar\Delta\tau}\right\} \quad (2)$$

After the propagation of the psips population by the set of random numbers Δx , a birth-disappearance step is performed according to the value of $V - V_{\text{ref}}$, where V_{ref} is a reference energy. The value of V_{ref} is adjusted after the move and the birth-disappearance step is performed for all psips. This adjustment is necessary to maintain the population number of psips approximately constant.

In this Article, we refer to a manifold M^d as a set of configuration points for a physical system.^{24,25,26} An Euclidean manifold is a configuration space that can be mapped faithfully (i.e., point by point) with a global set of mutually orthogonal axis. We use the symbol \mathbb{R}^d to represent a d -dimensional Euclidean space only if it is mapped with Cartesian coordinates throughout. Many important physical systems require non-Euclidean manifolds. Points in S^1 , the 2-dimensional sphere S^2 , the inertia ellipsoid (I^3) for the rotation of a non-linear top,²⁷ and toroids T^d (conformation space for d torsions) are traditionally mapped with angular variables. However, the ranges of these variables are open sets in \mathbb{R}^d ; therefore, these spaces cannot be considered Euclidean. S^2 and I^3 are examples of curved spaces, for which the Riemannian curvature scalar is a constant.

The spaces S^1 and T^d have zero scalar curvature but are non-Euclidean, non-simply connected spaces.

A number of complications arise in quantum mechanics when coordinates other than Cartesian are used. For example, the canonical quantization rules (in the position basis), for quantizing the momentum and position operators with Cartesian coordinates no longer apply in a non-Euclidean manifold.

The classical expression for the Hamiltonian in non-Euclidean manifolds is

$$\mathcal{H}(p,q) = \frac{1}{2} g^{\mu\nu} p_\mu p_\nu + V(q) \quad (3)$$

where $q = q^1, q^2, \dots, q^d$ is a configuration point in M^d . p_μ are the canonical conjugate momenta

$$p_\mu = \frac{\partial \mathcal{L}(q,\dot{q})}{\partial \dot{q}^\mu} \quad (4)$$

and $g^{\mu\nu}$ is the inverse of the metric tensor on M^d , an entity that contains all the geometric information for M^d , including the effective mass for the system (e.g., the moments of inertia if M^d is an inertia ellipsoid). In general, $g^{\mu\nu}$ depends on the configuration; therefore, if we attempt to use the canonical quantization rules directly, we produce operator ordering ambiguities.

A general quantization rule exists for all curvilinear and all non-Euclidean differentiable manifolds.²⁶ The time-dependent Schrödinger equation in a generic differential manifold M^d with metric tensor $g_{\mu\nu}$ is

$$-i\hbar \frac{\partial \psi}{\partial t} = \frac{\hbar^2}{2} \Delta_{LB} \psi - V\psi \quad (5)$$

where Δ_{LB} is the Laplace–Beltrami operator,

$$\Delta_{LB} = g^{\mu\nu} \partial_\mu \partial_\nu + g^{\mu\nu} [\partial_\mu \ln \sqrt{\det(g_{\mu\nu})}] \partial_\nu + (\partial_\mu g^{\mu\nu}) \partial_\nu \quad (6)$$

To develop diffusion Monte Carlo methods, we must now answer the following questions. How does diffusion take place on the surface of a sphere or on a general manifold? Further, how can one simulate such process numerically? One can construct quantum Monte Carlo (QMC) methods with non-Cartesian coordinates, but only a handful of publications on the subject can be found.^{8,28–32} It is possible to simulate diffusion numerically in manifolds. Perhaps the questions had been raised for the first time when the problem of quantizing in the curved space times of general relativity by using Feynman path integrals was first considered by DeWitt.³³ The DeWitt formalism is achieved by selecting to evaluate the classical action for the matrix element of the time evolution operator at the initial point of the slice q . DeWitt derives the form for the short-time evolution propagator matrix element; when this is converted by a Wick rotation to imaginary time propagation ($\tau = it$), it becomes

$$\begin{aligned} \langle q', \tau + \Delta\tau | q, \tau \rangle &= \left(\frac{1}{2\pi\hbar} \right)^{d/2} g'^{-1/4} D^{1/2}(q', \tau + \\ &\Delta\tau | q, \tau) g^{-1/4} \exp\left[-\frac{1}{\hbar} S(q', \tau + \Delta\tau | q, \tau)\right] \end{aligned} \quad (7)$$

where g is the determinant of the metric tensor evaluated at q : $g = \det[g_{\mu\nu}(q)]$. The action $S(q', \tau + \Delta\tau | q, \tau)$ is defined as the integral

$$S(q',\tau+\Delta\tau|q,\tau) = \int_{\tau}^{\tau+\Delta\tau} \mathcal{L}(q)d\tau \quad (8)$$

and $D(q',\tau+\Delta\tau|q,\tau)$ is the Van Vleck determinant $D = \det(D_{\mu\nu})$,

$$D_{\mu\nu} = -\frac{\partial^2 S}{\partial q^{\mu} \partial q^{\nu}} \quad (9)$$

If the action S and the Van Vleck determinant D are expanded about q, τ up to first order in $\Delta\tau$, one obtains an approximate expression for the matrix element of the time evolution operator

$$\langle q',\tau+\Delta\tau|q,\tau \rangle \approx \left[\frac{1}{2\pi\Delta\tau\hbar} \right]^{d/2} g^{1/2} \exp \left\{ -\frac{1}{2\hbar\Delta\tau} g_{\mu\nu} \Delta q^{\mu} \Delta q^{\nu} - \frac{1}{\hbar} \Delta\tau V \right\} \quad (10)$$

The potential energy V in this expression contains an additive quantum correction of order \hbar^2 proportional to the Riemannian curvature scalar.^{24,25} DeWitt derives this quantum correction term by forcing the expansion of the propagator in eq 10 to agree to first order with the Schrödinger equation in (5). The quantum correction to V can be safely ignored because all the manifolds that are of interest in the present Article have either a zero or constant curvature scalar.^{14–18}

The operator ordering issue shows itself as an infinite number of possible expansions of the time evolution operator. This freedom comes from the dependence of the metric tensor on configuration space, and the freedom to evaluate it at any point inside the time interval. Expanding the action at a particular point along the interval $[q',q]$ other than the initial point produces quantum correction terms to the potential that may be different from the Riemannian curvature scalar.

To use the DeWitt formula to derive quantum Monte Carlo algorithms, we need a global one-to-one map $\Phi: M^d \rightarrow \mathbb{R}^d$ so that nearly every point in M^d can be accessed by d independent coordinates $q = (q^1, \dots, q^\mu, \dots, q^d)$, and so that $-\infty < q^\mu < \infty \forall \mu$. We have found that this restriction on Φ is a sufficient condition to derive the Feynman–Kac equivalent in manifolds, which allows one to interpret the random fluctuation of all possible paths as a Brownian process. The same condition on M^d allows for the interpretation of the imaginary time evolution of an ensemble of replicas as a diffusion process; then we can replace the solution of one (the Schrödinger equation) with the simulation of the other (diffusion equation) in M^d . If in eq 10 we let $g_{\mu\nu}$ equal a diagonal matrix containing the masses of the physical particles, we obtain the usual DPL formula for finite temperature simulations in \mathbb{R}^d . The DMC step distribution for such case is the Gaussian in eq 2. Therefore, by analogy, the DeWitt quantization formula in eq 10 leads to the following generalization for the step distribution in M^d

$$W(q, \Delta q) = A \exp \left\{ -\frac{g_{\mu\nu} \Delta q^{\mu} \Delta q^{\nu}}{2\hbar\Delta\tau} \right\} \quad (11)$$

Our approach to develop a generalization of DMC for non-Euclidean manifolds is to perform a d -dimensional random walk on Δq to reproduce the distribution in eq 11 by a rejection technique. The “game of chance” first proposed by Anderson is unchanged but for one important detail; the distribution of steps to propagate the ensemble of replicas (or psips) is no longer Gaussian in general, unless the metric tensor is a constant independent of configuration. The approach employed to generate the random walk in Δq must satisfy detailed balance.

Mathematically, this is represented by the following equation:

$$W(q, \Delta q) T(\Delta q \rightarrow \Delta q') = W(q', \Delta q') T(\Delta q' \rightarrow \Delta q) \quad (12)$$

It should be noted that if we can drop the configuration dependence on W

$$W(\Delta q) T(\Delta q \rightarrow \Delta q') = W(\Delta q') T(\Delta q' \rightarrow \Delta q) \quad (13)$$

the random walk in Δq produces a Gaussian distribution for Δq . For the more general case, the reader should note that $q' \neq q + \Delta q$, and $q' \neq q + \Delta q'$ as one may be tempted to say at first. It is simple to verify that setting q' equal to either value would violate the detailed balance condition in eq 12. Therefore, eq 12 alone is insufficient to determine a unique algorithm. q and q' must be selected independently of $\Delta q'$. Yet, q and q' are not arbitrary; their physical meaning is the position of the psips in configuration space. Therefore, q and q' must be sampled from the ground state wavefunction as the DMC algorithm approaches convergence.

We choose the traditional uniform distribution for $T(\Delta q' \rightarrow \Delta q)$ by updating the value of Δq during the walk with

$$\Delta q' = \Delta q + \gamma(\eta - 0.5) \quad (14)$$

where η is a set of d uniformly distributed random numbers in $[0,1]$ and γ is a parameter that is adjusted to produce a 50% rejection rate. To satisfy all the requirements embodied in eq 12 and to account for the configuration dependence, we explore the following three choices, expressed in pseudo-code.

•Method 1:

Step 1: Draw d random numbers in $[0,1]$ and compute $\Delta q'$ with eq 14.

Step 2: Use q and Δq from the previous psip, and let q' be the configuration of the present psip.

Step 3: Compute the acceptance probability P for $\Delta q'$:

$$P = \min \left\{ 1, \exp \left[-\frac{g_{\mu\nu}(q') \Delta q'^{\mu} \Delta q'^{\nu}}{2\hbar\Delta\tau} + \frac{g_{\mu\nu}(q) \Delta q^{\mu} \Delta q^{\nu}}{2\hbar\Delta\tau} \right] \right\} \quad (15)$$

Step 4: Move the psip by $q' \rightarrow q' + \Delta q'$ if the move is accepted or by $q' \rightarrow q' + \Delta q$ if rejected.

Step 5: Set $\Delta q' \rightarrow \Delta q$ if the move is accepted, and repeat from Step 1 for all the psips.

•Method 2:

Step 1: Draw d random numbers in $[0,1]$ and compute $\Delta q'$ with eq 14.

Step 2: Use Δq from the previous psip, and let $q' = q$ be the configuration of the present psip.

Step 3: Compute the acceptance probability P for $\Delta q'$ using eq 15.

Step 4: Move the psip by $q' \rightarrow q' + \Delta q'$ if the move is accepted or by $q' \rightarrow q' + \Delta q$ if rejected.

Step 5: Set $\Delta q' \rightarrow \Delta q$ if the move is accepted and repeat from Step 1 for all the psips.

•Method 3:

Step 1: Draw d random numbers in $[0,1]$ and compute $\Delta q'$ with eq 14.

Step 2: Use Δq from the previous psip, let q be the position of the present psip, then draw another set of random numbers in $[0,1]$, and compute $q' = q + \gamma(\eta - 0.5)$. γ is the same as in eq 14.

Step 3: Compute the acceptance probability P for $\Delta q'$ with eq 15.

Step 4: Move the psip by $q' \rightarrow q' + \Delta q'$ if the move is accepted or by $q' \rightarrow q' + \Delta q$ if rejected.

Step 5: Set $\Delta q' \rightarrow \Delta q$ if the move is accepted and repeat from Step 1 for all the psips.

After all the psips are moved by either one of the methods above, the usual branching process is carried out using the potential energy surface.¹ Method 3 is a generalization of eq 12

$$W(q, \Delta q) T(\Delta q \rightarrow \Delta q') T(q \rightarrow q') = \\ W(q', \Delta q') T(\Delta q' \rightarrow \Delta q) T(q' \rightarrow q) \quad (16)$$

where $T(q \rightarrow q')$ is a uniform distribution. The walk is still only on $\Delta q'$, which is saved as Δq from move to move, whereas the value of q is reset for every psip moved to the initial position. Furthermore, the psip is moved by $\Delta q'$ if the move is accepted or by Δq if the move is rejected; the psip is never moved to q' .

Choosing q as the position of the psips to be moved is consistent with the DeWitt formula in all three strategies listed above. q is the “prepoint” at the moment that the time evolution operator is applied to the psips ensemble.

3. Numerical Tests

3.1. Particle in a Ring with a Non-confining External Potential. To distinguish between the traditional approach in Euclidean spaces and the present methods in manifolds, we compare simulations for the following two systems.

- (1) *A particle in S^1 with a unit radius.*
- (2) *A particle in \mathbb{R}^1 .*

All our quantities are expressed in atomic units. The mass of the particle is 207 au, and the potential energies V are identical for both systems:

$$V = V_0 \frac{4x}{x^2 + 4} \quad (17)$$

The potential function has a minimum value of $-V_0$ at $x = -2$, and a maximum of $+V_0$ at $x = +2$; V tends to zero at both asymptotes. The right-hand side of eq 17 transforms to $V_0 \cos \theta$ for the particle in a ring of unit radius if we interpret x as the stereographic projection coordinate for S^1 and we transform back to the angular variable. Therefore, the “exact” solution for the S^1 system can be obtained by diagonalizing the following Hamiltonian matrix, obtained by expanding Schrödinger’s equation in the free particle in a ring bases,

$$H_{ij} = \frac{\hbar^2}{2mR^2} \delta_{ij} + \frac{V_0}{2} (\delta_{ii+1} + \delta_{ii-1}) \quad (18)$$

The system in \mathbb{R}^1 can be easily solved with the discrete variable representation (DVR); we use the method developed by Colbert and Miller³⁴ to expand Schrödinger’s equation in the position vector space.

The two test systems are chosen with identical mass and potential energy parameters; $V_0 = 1$ hartree. Therefore, the zero point energy difference between them is a direct measure of the topological effects on the ground state. The ground state energy of the particle in a ring with $R = 1$ bohr and the particle in \mathbb{R}^1 with the same mass, and experiencing the same potential, can be found in the last row of Table 1. We experiment with several basis sizes (and cutoff values for the DVR computation) to produce the estimate of the truncation and cutoff errors associated with these two numbers. Despite our choice of unit radius, the ground state energy of the two test systems is significantly different.

The SPDMC simulations are carried out as follows: We perform a 10^6 move cycle to reach the asymptotic distribution.

TABLE 1: Ground State Energies for the Two Test Systems in Units of V_0

	S^1	\mathbb{R}^1
DMC, method 1	-0.9620 ± 0.0065	-0.9825 ± 0.0017
DMC, method 2	-0.9647 ± 0.0046	
DMC, method 3	-0.9639 ± 0.0053	
diagonalization	$-0.965399 \pm 1 \times 10^{-6}$	$-0.9828133 \pm 1 \times 10^{-6}$

The value of $\Delta\tau$ is 1.0×10^{-4} au for most of the simulations. We use an unusually small step size as part of our testing procedure because we are interested to learn whether the SPDMC methods can be impacted by possible quasiergodicity arising from the homotopy of the space.¹⁷ We make no attempt to optimize the step size because the system is of sufficiently small dimension to allow us to be as careful as possible in our comparison with diagonalization results. However, some simulations are repeated with $\Delta\tau = 1.0 \times 10^{-3}$ au for the purpose of comparing them with those that used a smaller step.

After the initial “warming” cycle, we run the simulation for another 10^6 moves over which we collect the energy and position data. For the particle in a ring, the psips are moved according to the random variable $\Delta\xi$, with distribution $W(z, \Delta\xi)$ equal to

$$W(z, \Delta\xi) = A \exp\left\{-\frac{8m}{(z^2 + 4)^2 \hbar \Delta\tau} (\Delta\xi)^2\right\} \quad (19)$$

A is a normalization constant, and z is the position of the psip before a move by $\Delta\xi$ is implemented. All three strategies presented in section 2 are tested. The psips are replicated or annihilated according to the value of $V - V_{\text{ref}}$ at the end of a move–branching cycle for all psips. The value of V_{ref} is adjusted to maintain the psip population count to 1000.

Without the configuration dependence, namely for \mathbb{R}^1 , eq 19 becomes

$$W(\Delta x) = A \exp\left\{-\frac{m}{2\Delta\tau} \Delta x^2\right\} \quad (20)$$

Therefore, the algorithms in section 2 are expected to produce, in the \mathbb{R}^1 case, a Gaussian distribution in Δx with the proper standard deviation $\sqrt{\Delta\tau/m}$. We use the rejection technique with the appropriate trivial modifications rather than using the usual Box–Muller algorithm. The preliminary work on \mathbb{R}^1 is a stepping stone toward the more complex algorithms proposed in section 2, and we use this approach to test our code.

For the S^1 case, the distribution of values of $\Delta\xi$ is non-trivial. In the course of the simulation we accumulate 10^7 values of $\Delta\xi$, and we analyze the distribution by creating 1000 bins between the largest and the smallest value of $\Delta\xi$. The result is graphed in Figure 1, where the histogram points are connected by a thin line. The $\Delta\xi$ distribution has a mean of zero, a standard deviation of 0.00172 bohr, and a skewness close to zero; however, it is leptokurtic. For ease of comparison, we draw in Figure 1 a Gaussian distribution with the same mean and standard deviation (thick line). Additionally, in Figure 1 we plot the step distribution for the same system in \mathbb{R}^1 (dashed line), for comparison with the other two distributions. The step distribution in S^1 is visibly broader than the Δx distribution in \mathbb{R}^1 for the identical system. Comparison between the thin and the thick lines in Figure 1 highlights the large difference in kurtosis between the distribution of eq 19 and a Gaussian distribution with equal mean and variance. For aesthetic reasons, we only graph the $\Delta\xi$ distribution for the first method. The other two methods produce distributions that are statistically identical to the one in Figure 1.

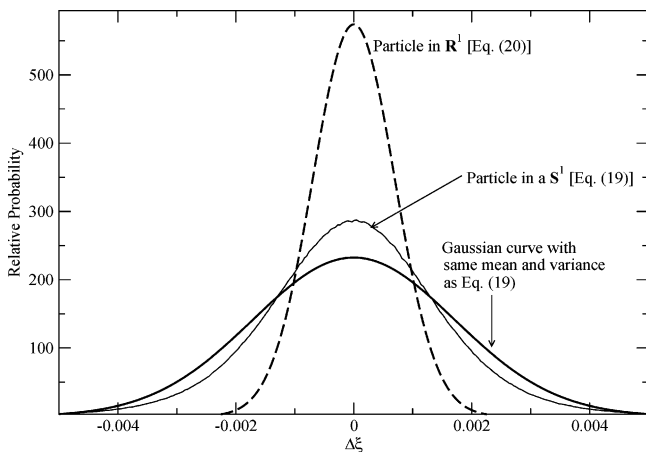


Figure 1. Comparison of the step distribution for the particle in a ring of unit radius (thin line), a Gaussian distribution of equal mean and variance (thick line), and the step distribution for the particle in a line with identical mass and potential energy (dashed line).

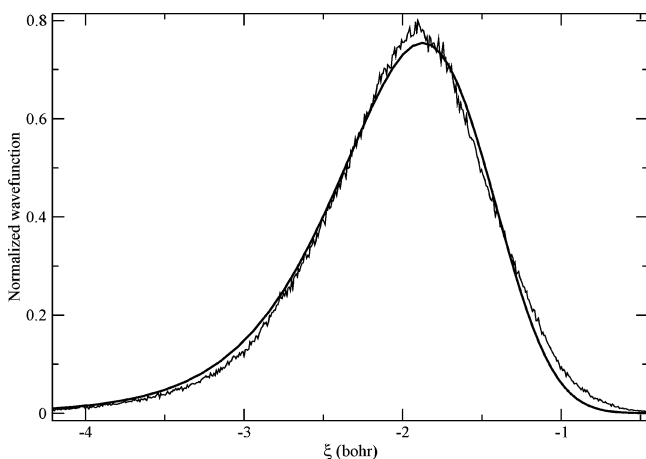


Figure 2. Comparison of the wavefunction obtained by diagonalization (thick line), with the histogram of psips positions generated by DMC (thin line), for the particle in a ring of unit radius.

The simulation of the particle in a ring with all three methods yields the ground state energies tabulated in the second column of Table 1. The error tabulated in the same column is 1.982 times the standard deviation. All three are equal to each other and to the diagonalization value within the statistical error. Furthermore, all three values are significantly different from the ground state energy obtained with the same mass and potential in R^1 . The value of the energy reported in Table 1 for method 2 is obtained with $\Delta\tau = 1.0 \times 10^{-3}$ au.

We also compare the ground state wavefunctions. For all the SPDMC simulations, we collect all the positions of the psips population every 1000 moves. This produces a sample containing roughly 10^6 values of ξ . The resulting distributions are compared against the ground state obtained by diagonalization. The results for the particle in a ring (using method 1) are graphed in Figure 2. The thick line in Figure 2 is obtained by plotting

$$\left[\frac{1}{\sqrt{2\pi}} \sum_{n=-\infty}^{\infty} c_n \cos(n\theta) \right] \frac{4}{\xi(\theta)^2 + 4} \quad 0 < \theta < 2\pi \quad (21)$$

versus $\xi(\theta)$. The numbers c_n are the entries of the ground state eigenvector in the free ring basis obtained by the diagonalization of the Hamiltonian matrix in eq 18. The abscissa is

$$\xi(\theta) = \frac{2 \cos \theta}{1 - \sin \theta} \quad (22)$$

and the factor $4/[\xi(\theta)^2 + 4]$ outside the square brackets in eq 21 is needed to transform $\Delta\theta$ to $\Delta\xi$ so that the ground state wavefunction obtained with the angular coordinate can be compared with the histogram generated by the SPDMC simulations. The histograms generated from all three SPDMC simulations are statistically identical; therefore, we only present the one produced by method 1. For the particle in Euclidean space, the rejection method to produce a Gaussian distribution for Δx together with the usual branching process from the potential term yields the ground state energy tabulated in the second row, third column of Table 1. This value is also in excellent agreement with the DVR value, found in the same column, in the bottom row. Finally, in Figure 3 we compare the wavefunction obtained by the DVR of Colbert and Miller, and the histogram of psips positions accumulated during the DMC simulation.

3.2. Coulomb Problem with the Rotational Barrier. Let us consider the following remapping of the three-dimensional Euclidean space,

$$\begin{aligned} x &= \exp(-\xi) \sin \theta \cos \phi \\ y &= \exp(-\xi) \sin \theta \sin \phi \\ z &= \exp(-\xi) \cos \theta \end{aligned} \quad (23)$$

where θ and ϕ are the familiar spherical polar angles and $\exp(-\xi)$ replaces the radial coordinate. It should be noted that the partitioning $\Phi: R^3 \rightarrow R^+ \otimes S^2$ is achieved, but R^+ is remapped: $\Phi: R^3 \rightarrow R^+ \otimes S^2 \rightarrow R^1 \otimes S^2$. The subspace S^2 is not remapped with stereographic projections, because the algorithms are applied to a one-dimensional isotropic problem, for which the variables θ and ϕ are cyclic. Using the transformation law for the metric

$$g_{\mu\nu} = \frac{\partial x^{\mu'}}{\partial x^\mu} \frac{\partial x^{\nu'}}{\partial x^\nu} g_{\mu'\nu'} \quad (24)$$

and using $g_{\mu'\nu'} = \delta_{\mu'\nu'}$ for the Euclidean metric in R^3 , one derives in a straightforward way the following expression

$$g_{\mu\nu} = \exp(-2\xi) \begin{pmatrix} 1 & 0 & 0 \\ 0 & \sin^2 \theta & 0 \\ 0 & 0 & 1 \end{pmatrix} \quad (25)$$

Thus, the classical Hamiltonian for a particle of mass m in an isotropic potential becomes

$$\mathcal{H} = \frac{1}{2m} \exp(2\xi) \left(p_\theta^2 + \frac{p_\phi^2}{\sin^2 \theta} + p_\xi^2 \right) + V(\xi) \quad (26)$$

whereas, the Laplace–Beltrami operator²⁶ takes the following form

$$\nabla^2 = \exp(2\xi) \left(\frac{\partial^2}{\partial \theta^2} + \frac{1}{\sin^2 \theta} \frac{\partial^2}{\partial \phi^2} + \frac{\cos \theta}{\sin \theta} \frac{\partial}{\partial \theta} + \frac{\partial^2}{\partial \xi^2} - \frac{\partial}{\partial \xi} \right) \quad (27)$$

The first three terms inside the parentheses constitute the angular momentum operator \mathbf{L}^2 . Because V only depends on ξ , we expand with spherical harmonics, left multiply by the complex conjugate of the basis, and integrate over the solid angle. The result is the following Hamiltonian operator (in atomic units)

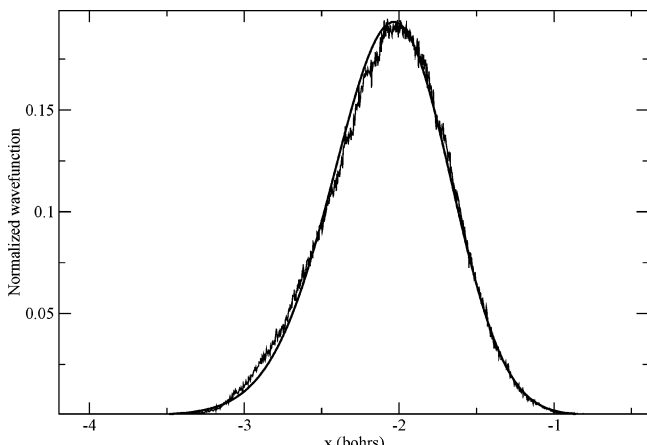


Figure 3. Comparison of the DVR wavefunction (thick line), with the histogram of psips positions generated by DMC (thin line), for the particle in \mathbb{R}^1 . The mass and the potential energy model are identical to those used to generate the graph in Figure 2.

$$\mathbf{H} = -\frac{1}{2m} \exp(2\xi) \left(\frac{\partial^2}{\partial \xi^2} - \frac{\partial}{\partial \xi} \right) + \frac{l(l+1)}{2m} \exp(2\xi) + V(\xi) \quad (28)$$

This is the differential equation that one solves by DMC, with $m = 1$, $V(\xi) = -\exp(\xi)$, the Coulomb potential, and with $l > 0$. The classical imaginary time Lagrangian for this one-dimensional problem is

$$\mathcal{L} = \frac{1}{2} \exp(-2\xi) \dot{\xi}^2 - \frac{l(l+1)}{2} \exp(2\xi) - \exp(\xi) \quad (29)$$

Therefore, a random walk is performed to produce the following $\Delta\xi$ distribution

$$\exp\left\{-\frac{1}{2\Delta\tau} \exp(-2\xi)(\Delta\xi)^2\right\} \quad (30)$$

Simulations comprising 10^6 moves are performed for several values of l , using a $\Delta\tau = 2.0 \times 10^{-3}$ atomic units and $N = 1000$. The wavefunction obtained with a given value of l corresponds to the $l = n - 1$ Rydberg states of the hydrogen atom and is nodeless of course. The energies obtained with method 2 are compared against $E_n = -2^{-1}n^{-2}$ in Table 2. It is clear in Figure 4 that the step distribution for the exponent ξ is not Gaussian.

3.3. Ground State of a Rigid Asymmetric Top. To demonstrate the usefulness of the methods, we consider the following low-dimensional but non-trivial example. Let I_λ ($\lambda = 1, 2, 3$) represent the eigenvalues of the moment of inertia tensor, then the appropriate metric tensor for a rigid top is

$$g_{\mu\nu} = I_\lambda J_\mu^{\mu'} J_\nu^{\nu'} f_{\mu'\nu'}^\lambda \quad (31)$$

where the symbol $f_{\mu\nu}^\lambda$ represents a set of eighteen independent functions obtained by writing the kinetic energy of a rigid asymmetric top in the center of mass frame in terms of the Euler angles θ, ϕ, ψ . The functions $f_{\mu\nu}^\lambda$ expressed with Euler angles can be found in classical mechanics textbooks.²⁵

$$f_{11}^1 = \cos^2 \psi \quad (32)$$

$$f_{11}^2 = \sin^2 \psi \quad (33)$$

TABLE 2: Energies for the $l = n - 1$ Rydberg States (Hartree)

l	n	E_n	DMC (method 2)
1	2	-0.12500	-0.145464 ± 0.032188
2	3	-0.05555	-0.056925 ± 0.004448
3	4	-0.03215	-0.031511 ± 0.001454
4	5	-0.02000	-0.020148 ± 0.000673
5	6	-0.01388	-0.013955 ± 0.000371
6	7	-0.01020	-0.010275 ± 0.000336
7	8	-0.00781	-0.007881 ± 0.000085
8	9	-0.00617	-0.006172 ± 0.000068
9	10	-0.00500	-0.005028 ± 0.000061
10	11	-0.00413	-0.004116 ± 0.000066

$$f_{12}^1 = f_{21}^1 = -f_{12}^2 = -f_{21}^2 = \sin \theta \cos \psi \sin \psi \quad (34)$$

$$f_{22}^1 = \sin^2 \theta \sin^2 \psi \quad (35)$$

$$f_{22}^2 = \sin^2 \theta \cos^2 \psi \quad (36)$$

$$f_{22}^3 = \cos^2 \theta \quad (37)$$

$$f_{23}^3 = \cos \theta \quad (38)$$

$$f_{33}^3 = 1 \quad (39)$$

The symbol $J_\mu^{\mu'}$ represents the Jacobian matrix element for the transformation between the Euler angle $q^{\mu'}$ and the stereographic projection q^μ . The $\xi^1, \xi^2, \xi^3 \rightarrow \theta, \phi, \psi$ map is

$$\theta = 2 \sin^{-1} \sqrt{\frac{(4\xi^2)^2 + (4\xi^3)^2}{(\xi^1)^2 + (\xi^2)^2 + (\xi^3)^2 + 4}} \quad (40)$$

$$\phi = \tan^{-1} \left(\frac{(\xi^1)^2 + (\xi^2)^2 + (\xi^3)^2 - 4}{4\xi^1} \right) - \tan^{-1} \left(\frac{\xi^3}{\xi^2} \right) \quad (41)$$

$$\psi = \tan^{-1} \left(\frac{(\xi^1)^2 + (\xi^2)^2 + (\xi^3)^2 - 4}{4\xi^1} \right) + \tan^{-1} \left(\frac{\xi^3}{\xi^2} \right) \quad (42)$$

These expressions can be easily inverted,

$$\xi^1 = \cos \frac{\theta}{2} \cos \frac{\phi + \psi}{2} \begin{cases} \frac{1 + \cos \frac{\theta}{2} \sin \frac{\phi + \psi}{2}}{1 - \cos \frac{\theta}{2} \sin \frac{\phi + \psi}{2}} + 1 \end{cases} \quad (43)$$

$$\xi^2 = \sin \frac{\theta}{2} \cos \frac{\phi - \psi}{2} \begin{cases} \frac{1 + \cos \frac{\theta}{2} \sin \frac{\phi + \psi}{2}}{1 - \cos \frac{\theta}{2} \sin \frac{\phi + \psi}{2}} + 1 \end{cases} \quad (44)$$

$$\xi^3 = \sin \frac{\theta}{2} \sin \frac{\phi - \psi}{2} \begin{cases} \frac{1 + \cos \frac{\theta}{2} \sin \frac{\phi + \psi}{2}}{1 - \cos \frac{\theta}{2} \sin \frac{\phi + \psi}{2}} + 1 \end{cases} \quad (45)$$

We use geometric arguments similar to those for \mathbb{S}^1 to derive the map and its inverse from Eulerian angles to the stereographic projections by using the four-dimensional quaternion space and the spherical constraint. To simplify the notation further, we introduce seven auxiliary quantities

$$d^1 = \sqrt{16(\xi^1)^2 + [(\xi^2)^2 + (\xi^3)^2 + 4]^2} \quad (46)$$

$$d^2 = \sqrt{(\xi^2)^2 + (\xi^3)^2} \quad (47)$$

$$d^3 = (d^2)^2 \quad d^4 = (d^1)^2 \quad (48)$$

$$d^5 = 8(\xi^1)^2 - 4[(\xi^1)^2 + (\xi^2)^2 + (\xi^3)^2 - 4] \quad (49)$$

$$d^6 = -(\xi^1)^2 + (\xi^2)^2 + (\xi^3)^2 + 4 \quad (50)$$

$$d^7 = (\xi^1)^2 + (\xi^2)^2 + (\xi^3)^2 - 4 \quad (51)$$

Then the Jacobian is

$$J_{\mu'}^{\mu} = \begin{pmatrix} -\frac{16d^2\xi^1}{d^1d^6} & \frac{2d^5\xi^2}{d^1d^2d^6} & \frac{2d^5\xi^3}{d^1d^2d^6} \\ \frac{d^5}{d^4} & \frac{8\xi^1\xi^2}{d^4} + \frac{\xi^3}{d^3} & \frac{8\xi^1\xi^3}{d^4} - \frac{\xi^2}{d^3} \\ \frac{d^5}{d^4} & \frac{8\xi^1\xi^2}{d^4} - \frac{\xi^3}{d^3} & \frac{8\xi^1\xi^3}{d^4} + \frac{\xi^2}{d^3} \end{pmatrix} \quad (52)$$

and the non-vanishing $f_{\mu'\nu'}^{\lambda}$ functions are

$$f_{11}^1 = \left(\frac{4\xi^1\xi^2 - \xi^3 d^7}{d^1 d^2} \right)^2 \quad (53)$$

$$f_{11}^2 = \left(\frac{4\xi^1\xi^3 + \xi^2 d^7}{d^1 d^2} \right)^2 \quad (54)$$

$$f_{12}^1 = f_{21}^1 = -f_{12}^2 = -f_{21}^2 = \frac{8(4\xi^1\xi^2 - \xi^3 d^7)(4\xi^1\xi^3 + \xi^2 d^7)}{(d^6)^2 d^1 d^2} \quad (55)$$

$$f_{22}^1 = \frac{64(4\xi^1\xi^3 + \xi^2 d^7)}{(d^6)^4} \quad (56)$$

$$f_{22}^2 = \frac{64(4\xi^1\xi^2 - \xi^3 d^7)}{(d^6)^4} \quad (57)$$

$$f_{22}^3 = \left[\frac{2d^4}{(d^6)^2} - 1 \right]^2 \quad (58)$$

$$f_{23}^3 = f_{32}^3 = \frac{2d^4}{(d^6)^2} - 1 \quad (59)$$

$$f_{33}^3 = 1 \quad (60)$$

Clearly, $g_{\mu\nu}$ is analytical; however, expressing its elements as functions of ξ^v does not provide any additional insight. Therefore, we simply evaluate $f_{\mu'\nu'}^{\lambda}$ and $J_{\mu'}^{\mu}$ separately and translate the sum in eq 31 directly into code.

The eigenvalues of the inertia tensor I_{λ} are chosen to be identical to those of rigid water, namely, $I_x, I_y, I_z \approx 12614, 8588, 4026$ atomic units, respectively. The rotations are hindered using an external scalar field represented by the function

$$V(\xi^1, \xi^2, \xi^3) = -V_0 \frac{\xi^1 + \xi^2 + \xi^3}{(\xi^1)^2 + (\xi^2)^2 + (\xi^3)^2 + 4} \quad (61)$$

The value of V_0 is 0.04 hartree. The potential energy models a non-trivial sinusoidal external field when expressed in terms of the Eulerian angles. V is symmetric under the exchanges $\xi^{\mu} \rightarrow \xi^{\nu}$; therefore, it is simple to find the direction (i.e., $y = \xi^1 = \xi^2 = \xi^3$) along which both the maximum and the minimum $\pm \sqrt{3}V_0/4$ exist. These are at $(\xi^1 = \xi^2 = \xi^3 = -\sqrt{4/3})$ and $(\xi^1 = \xi^2 = \xi^3 = +\sqrt{4/3})$ respectively. The results of the SPDMC

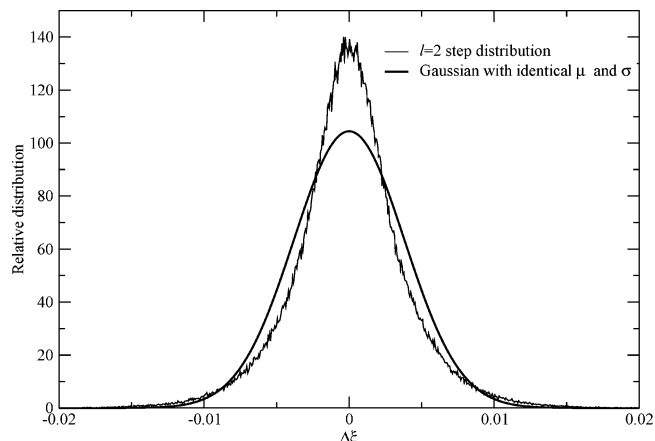


Figure 4. Steps distribution for the electron in the field of an infinitely massive proton (thin line), compared with a Gaussian distribution of equal mean and variance (thick line).

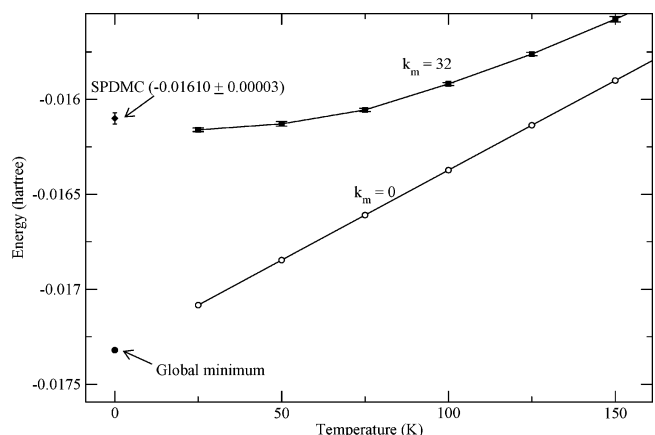


Figure 5. Energies of a rigid water molecule in an external field.

simulations are presented in Figure 5. The global minimum with $V_0 = -0.04$ hartree is -0.0173205 hartree. The ground state energy (-0.01610 ± 0.00002 hartree) is substantially greater than the global minimum and is statistically indistinguishable from the finite temperature average energy at 50 K obtained by stereographic projection path integral.¹⁶

4. Discussion

This Article introduces a new set of algorithms for the DMC simulation in differential manifolds that can be mapped onto the equidimensional Euclidean space. We make use of stereographic projections for spaces that are combinations of S^1, S^2, I^3 , and T^d , and we develop a logarithmic bijection for the remapping of \mathbb{R}^+ . The numerical tests confirm that one can develop a variety of SPDMC algorithms to find ground state energies and wavefunctions in key differential manifolds provided a faithful mapping $M^d \rightarrow \mathbb{R}^d$ is available. The procedures are very similar to the original one; the only difference is the process used to generate the steps by which to move replicas. The non-Gaussian distribution of the steps arises from the configuration dependence of the metric tensor. Three different methods that satisfy detailed balance to generate random numbers with the appropriate distribution are tested.

The particle in S^1 has a significantly different ground state energy and wavefunction compared to a particle in \mathbb{R}^1 with identical mass and potential energy. The step size distribution for the particle in S^1 has a variance larger than the step size distribution for the identical systems in \mathbb{R}^1 . Furthermore, the distribution is narrower than a Gaussian distribution of the same

variance but symmetric about the mean of zero. All the numerical tests are in excellent agreement with the results obtained analytically or by diagonalization. All three algorithms we implement to generate the non-Gaussian distribution of the steps produce statistically identical results. We learn that the difference between q and q' is arbitrary, as long as the values of either q or q' are sampled from the correct position distribution.

An external *non-confining* potential energy surface for the particle in a ring is chosen to make our test as stringent as possible. It is very important to test stochastic algorithms for non-Euclidean spaces with non-confining potentials, because routine assumptions regarding space boundaries do not apply, leading to catastrophic failures.¹⁵ Although most torsional degrees of freedom are hindered, the tumbling of rigid bodies is not confined in general; thus it is important to design careful tests to ensure the methods are applicable to complex problems in condensed matter physics. Therefore, the algorithms are subjected to very stringent tests with external non-confining potentials. Unlike other non-Euclidean spaces, the set of points in a ring (or any higher dimensional toroid) is not a simply connected space. In contrast, the Haldene sphere used in ref 23 is a simply connected space. Therefore, this Article is the first to demonstrate that the use of projective bijections allows for the construction of SPDMC algorithms in non-simply connected manifolds. In our simulations in the particle in a ring space, we make use of unusually small time steps to learn whether or not the homotopy of the space generates any quasiergodicity in the DMC random walk. As we have explained, the particle in a ring, though seemingly trivial, is a multiply connected space: A particle in a ring can move from ϕ_a to ϕ_b in an infinite number of ways; it can take a direct path moving counterclockwise, or it can get there by moving around the ring any number of times (windings) in the clockwise direction, and then winding around the ring any number of times in the counterclockwise direction before stopping at ϕ_b . One of the reasons why angular variables do not work like Cartesian coordinates to simulate diffusion in such complicated spaces is one must impose special boundary conditions and keep track of the windings that have taken place. These subtleties become important when non-confining potentials are used. It is not an easy task to incorporate these requirements into the implementations of Monte Carlo methods, though some authors have reported success along these lines (e.g., ref 32). The crux of the methods we propose in the present Article is to remap this space by using a “Cartesian-like” coordinate (the stereographic projection) so that the issue of imposing boundary conditions and the homotopy issue disappear in the implementation of the quantum methods. However, as we have learned in previous work, all the characteristics of the space are still there and sometimes show up as numerical difficulties such as quasiergodic behavior in what should be a “straightforward” one-dimensional problem. In using such a small step size we ensure ourselves that no such numerical difficulty is encountered in our numerical tests when a non-confining potential energy surface (typical of what one finds in condensed matter applications), is used. It turns out that these difficulties are not present in what may at first appear as a much more formidable problem of simulating diffusion on the inertia ellipsoid, as in our third example. Nevertheless, the particle in a ring space finds many applications in condensed molecular physics (e.g., rotations on a surface), and any proclaimed new methods to handle holonomic constraints should be made to meet this important benchmark. The three methods we introduce

here can be easily generalized to systems with larger dimensions, such as a cluster of rigid non-linear molecules.

Of course, the first two examples have been chosen because it is possible to solve them in a number of different ways. In particular, the following applies for the electron in the field of a proton: Even with the map used here, namely $r = \exp(-\xi)$, one cannot simulate the $l = 0$ case given the negative singularity of the Coulomb potential for that case. The walkers constantly drift to larger values of ξ forced by deeper values of V_{ref} at every iteration. The problem could be solved by using an artificial barrier that accounts for a finite size of the proton. Alternatively, one could employ the elegant machinery of the Duru–Kleinert transformation to stabilize the source near the singularity of the potentials. This approach has led to the analytic solution of the three-dimensional Coulomb problem by path integrals.²⁶ However, the use of the Duru–Kleinert transformation to stabilize stochastic simulations around singular potentials has never been attempted. Because the Coulomb potential with a rotational barrier is confining (i.e., it prevents moves taking walkers to negative values of r), the DMC algorithms could have sampled r as the independent variable for the configuration. Furthermore, one could run the DMC algorithm with r as the independent variable and with a \dot{r} , sampled from a Gaussian distribution: It is well-known that the transformation of dependent variables $rR(r) = P(r)$ produces a Laplace–Beltrami operator for \mathbb{R}_+ equal to the Laplacian in \mathbb{R}^1 . The hydrogen atom is a simple and familiar example of a coset space not generated by the imposition of constraints.

There exist other possibilities to develop SPDMC methods in manifolds that are not pursued here. One clear alternate approach would be the extension of the ground state path integral method recently proposed by Sarsa et al.³⁵ Because their scheme relies entirely on DPI simulations, it would be straightforward to apply the DeWitt formula directly to their algorithm. A less rigorous, but perhaps equally functional, approach could be obtained by modifying the Langevin equation; one would add the following drift terms

$$\int_{\tau}^{\tau+\Delta\tau} \Gamma_{\lambda\nu}^{\mu} \dot{q}^{\nu} \dot{q}^{\lambda} d\tau \approx \Gamma_{\lambda\nu}^{\mu} \frac{\Delta q^{\nu} \Delta q^{\lambda}}{\Delta\tau} \quad (62)$$

to the regular random Gaussian process. The quantities symbolized by $\Gamma_{\lambda\nu}^{\mu}$ are the Christoffel connections of the second kind,^{24–26}

$$\Gamma_{\lambda\nu}^{\mu} = \frac{1}{2} g^{\mu\rho} (\partial_{\lambda} g_{\nu\rho} + \partial_{\nu} g_{\rho\lambda} - \partial_{\rho} g_{\lambda\nu}) \quad (63)$$

The terms in the integrand of eq 62 can be interpreted as the forces of constraint; these can be obtained without any assumption about their nature, and without the need to compute Lagrange multipliers. Assuming such an approach works, it could be used to study alternative theories based on the expansion point of the time evolution operator. For example, one could choose to evaluate $g_{\mu\nu}$ and $\Gamma_{\lambda\nu}^{\mu}$ at the midpoint between q and $q + \Delta q$, because these quantities would be known with this scheme before the move; the resulting approach would be consistent with the Weyl expansion of the time evolution operator.³⁶

Acknowledgment is made to the donors of the Petroleum Research Fund, administered by the ACS (grant number 40946-B6) for partial support of this research. Support is also gratefully acknowledged from The Stacy Ann Vitetta '82 Professorship

Fund, and The Ellington Beavers Fund for Intellectual Inquiry at Arcadia University.

References and Notes

- (1) Anderson, J. B. *J. Chem. Phys.* **1975**, *63*, 1499.
- (2) Ceperley, D. M.; Alder, D. *Science* **1986**, *231*, 555.
- (3) Ceperley, D. M.; Alder, B. *J. J. Chem. Phys.* **1984**, *81*, 5834.
- (4) Lester, W. A., Jr.; Hammond, B. L. *Annu. Rev. Phys. Chem.* **1990**, *41*, 283.
- (5) Reynolds, P. J.; Ceperley, D. M.; Alder, B. J.; Lester, W. A., Jr. *J. Chem. Phys.* **1982**, *77*, 1378.
- (6) Buch, V. *J. Chem. Phys.* **1992**, *97*, 726.
- (7) Sarsa, A.; Schmidt, K. E.; Moskowitz, J. W. *J. Chem. Phys.* **2000**, *113*, 44.
- (8) Clary, D. C. *J. Chem. Phys.* **2001**, *114*, 9725.
- (9) Lewerenz, M. *J. Chem. Phys.* **1996**, *104*, 1028.
- (10) Sun, H.; Watts, R. O. *J. Chem. Phys.* **1990**, *92*, 603.
- (11) Sandler, P.; Oh, Jung, J.; Szczęśniak, M. M.; Buch, V. *J. Chem. Phys.* **1994**, *101*, 1378.
- (12) Lee, H.-S.; Herbert, J. M.; McCoy, A. B. *J. Chem. Phys.* **1999**, *110*, 5481.
- (13) Sandler, P.; Buch, V.; Sadlej, J. *J. Chem. Phys.* **1996**, *105*, 10387.
- (14) Curotto, E. *J. Chem. Phys.* **2005**, *123*, 134102.
- (15) Russo, M. F., Jr.; Curotto, E. *J. Chem. Phys.* **2003**, *118*, 6806.
- (16) Russo, M. F., Jr.; Curotto, E. *J. Chem. Phys.* **2004**, *120*, 2110.
- (17) Avilés, M. W.; Curotto, E. *J. Chem. Phys.* **2005**, *122*, 164109.
- (18) Unpublished results.
- (19) Jiang, H.; Xu, M. Z.; Hutson, J. M.; Baćić, Z. *J. Chem. Phys.* **2005**, *123*, 054305.
- (20) Jiang, H.; Baćić, Z. *J. Chem. Phys.* **2005**, *122*, 244306.
- (21) Paesani, F.; Gianturco, F. A.; Whaley, K. B. *J. Chem. Phys.* **2001**, *115*, 10225.
- (22) Moskowitz, J. W.; Baćić, Z.; Sarsa, A.; Schmidt, K. E. *J. Chem. Phys.* **2001**, *114*, 10294.
- (23) M-Alaverdian, V.; Bonesteel, N. E.; Ortiz, G. *Phys. Rev. Lett.* **1997**, *79*, 5286.
- (24) Schutz, B. *A First Course in General Relativity*; Cambridge Press: New York, 1985.
- (25) Curtis, W. D.; Miller, F. R. *Differential Manifolds and theoretical physics*; Academic Press: New York, 1985.
- (26) Kleinert, H. *Path integrals in Quantum Mechanics, Statistics and Polymer physics*; World Scientific: Singapore, 1990.
- (27) Rosenthal, G. *J. Phys. A. Math. Gen.* **2001**, *34*, L169.
- (28) Kuharski, R. A.; Rossky, P. J. *J. Chem. Phys.* **1985**, *82*, 5164.
- (29) Marx, D.; Müser, M. H. *J. Phys. Condens. Matter.* **1999**, *11*, R117.
- (30) Marx, D.; Nielaba, P. *Phys. Rev. A.* **1992**, *45*, 8968.
- (31) Miller, T. F., III; Clary, D. C. *J. Chem. Phys.* **2003**, *119*, 68.
- (32) Clary, D. C. *J. Chem. Phys.* **2002**, *116*, 8262.
- (33) DeWitt, B. S. *Rev. Mod. Phys.* **1957**, *29*, 377.
- (34) Colbert, D. T.; Miller, W. H. *J. Chem. Phys.* **1992**, *96*, 1982.
- (35) Sarsa, A.; Schmidt, K. E.; Magro, W. R. *J. Chem. Phys.* **2000**, *113*, 1366.
- (36) Mizrahi, M. M. *J. Math. Phys.* **1975**, *16*, 2201.